Journal of Alloys and Compounds, 203 (1994) 67–75
JALCOM 857

Thermal conductivity and specific heat of boron carbides

P.A. Medwick, H.E. Fischer* and R.O. Pohl
Laboratory of Atomic and Solid State Physics, Cornell University, Ithaca, NY 14853-2501 (USA)

(Received June 1, 1993)

Abstract

We present measurements of the thermal conductivity ($30 < T < 300$ K) and specific heat ($80 < T < 300$ K) of *polycrystalline* boron carbides ($B_{1-x}C_x$) for carbon concentrations spanning the single-phase field ($0.1 < x < 0.2$) and compare our results with studies in other temperature regimes. The thermal conductivity decreases continuously with decreasing x as it evolves from crystalline behavior for carbon-rich specimens to a glass-like conductivity characteristic of *amorphous* solids. The specific heat of boron carbides is insensitive to the carbon concentration for $T > 60$ K.

1. Introduction

Boron carbides ($B_{1-x}C_x$) possess unique structural, electronic and thermal properties. Owing to their extreme hardness, they have historically been used as abrasives and armor [1]. The large neutron capture cross-section of the ^{10}B nucleus has also led to their use as control elements in nuclear reactors [2]. More recently, the use of boron carbides in high temperature thermoelectric generators has become attractive owing to their mechanical robustness, high melting points and substantial thermopowers [3]. As a result, efforts have been made to maximize the thermoelectric figure-of-merit $Z = S^2\sigma/\Lambda$, where S is the Seebeck coefficient, σ is the electrical conductivity and Λ is the thermal conductivity [3]. It is therefore important to know the lowest attainable thermal conductivity of these materials. Prior studies have indicated that the thermal conductivity is sensitive to the carbon content of the lattice but have not produced a clear answer to the question of its lowest value. In order to clarify this issue, we measured the thermal conductivity of boron carbides for various carbon compositions over the single-phase region ($0.1 < x < 0.2$). Our results show that the thermal conductivity evolves from crystalline to glass-like behavior as carbon is removed from the lattice. The thermal conductivity decreases continuously with decreasing carbon content and approaches a limiting value at high temperatures. In addition, we report measurements of the specific heat of boron carbide which illustrate that the specific heat is insensitive to x for $T > 60$ K.

2. Structure of boron carbides

$B_{1-x}C_x$ exists as a single crystallographic phase for carbon concentrations between approximately 9 and 20 at.%, although there is some disagreement over the precise boundaries of the single-phase field [4–6]. The crystal structure of boron carbide is a modification of the α-B structure. The unit cell of α-B is rhombohedral with lattice parameter $a = 5.19$ Å and vertex angle $\alpha = 65°18'$ [7]. The lattice constants of boron carbides are sensitive functions of their carbon content as well as the presence of impurities [8]. In $B_{1-x}C_x$, slightly deformed boron-rich icosahedra are centered at each vertex of the rhombohedron. Each icosahedron has 12 externally directed bonds emanating from it. Six of these bonds join atoms in a given icosahedron to their counterparts in the six neighboring icosahedra along the edges of the rhombohedral cell. The remaining six bonds join icosahedral atoms to end atoms of a three-member chain within each rhombohedral cell. These so-called intericosahedral chains are directed along the long body diagonal (threefold axis) of the unit cell. Studies to date suggest that the primary configurations of the intericosahedral chains are carbon–boron–carbon (CBC) and carbon–boron–boron (CBB) depending upon the carbon content of the sample [9]. It is generally recognized that the microscopic arrangement of boron and carbon is *uniquely* determined by the stoichiometry of the sample rather than resulting from randomly

*Present address: LURE, Bâtiment 209D, Centre Universitaire Paris-Sud, F-91405 Orsay Cedex, France.

SSDI 0925-8388(93)00857-U

populating *arbitrary* atomic sites with boron and carbon in order to achieve the correct stoichiometry. Rather, boron and carbon atoms preferentially populate either the icosahedra or the intericosahedral chains as dictated by the overall carbon content of the lattice. However, despite this regularity, the boron carbides still retain a form of compositional disorder as we discuss below.

Emin has developed a microscopic description of the boron carbide structure [10]. In this picture the structure at the carbon-rich end of the single-phase field is envisioned to consist of $B_{11}C$ icosahedra centered at the unit cell vertices with CBC intericosahedral chains. This limit is believed to correspond to a composition near, but slightly less than, 20 at.%. For ease of notation we will hereafter refer to the carbon-saturated limit as "$x=0.2$" and "B_4C". We wish to emphasize that this notation is a formalism which is meant to indicate the carbon-rich limiting composition. Although the carbon-saturated material is composed entirely of $B_{11}C$ icosahedra and CBC chains, there is still some disorder in the lattice associated with the random placement of a single carbon atom amongst many sites within a particular icosahedron. For carbon-unsaturated specimens it is suggested that carbon atoms are first preferentially removed from the intericosahedral chains, thereby converting CBC configurations to CBB. This process also introduces additional lattice disorder, since only enough CBC chains are randomly converted to CBB chains in order to achieve a particular overall carbon concentration. The CBC→CBB process continues until all the three-membered chains have been converted to CBB chains at an overall carbon concentration of $x=0.133$. As x continues to decrease, carbon atoms are then removed from some of the icosahedra, thereby driving the process $B_{11}C \rightarrow B_{12}$ until the lower limit of the single-phase field is reached. However, even at the carbon-poor limit of the phase field, some $B_{11}C$ icosahedra will still be present in the lattice. Such a microscopic description of the boron carbide lattice has been shown to be in good agreement with existing structural, acoustic, electrical and thermal data [11].

3. Experimental details

3.1. Thermal conductivity

The samples used in our thermal conductivity measurements were prepared by Dr. T. Aselage at Sandia National Laboratories by hot pressing ($T=2450$ K, $P=6000$ lbf in^{-2}) a mixture of boron and graphite powders under an argon atmosphere in a graphite die lined with boron nitride [12]. The crystalline boron powder was approximately 97% enriched in ^{11}B and had a particulate size of less than 150 μm; the particulate size of the graphite powder is unknown [13]. Additional details are given in ref. 12. Grain sizes of the resulting polycrystalline samples were approximately 10–20 μm for carbon-rich samples ($x \approx 0.2$) and 50–60 μm for carbon-poor samples ($x \approx 0.1$) [13]. The carbon contents of the three measured samples were $x=0.1$, 0.133 and 0.2. Their mass densities were $\rho=2.45$, 2.49 and 2.55 g cm^{-3} respectively [13]. In Table 1 an estimate of the theoretical density for each composition assuming 100% ^{11}B and 100% ^{12}C enrichment and using unit cell volumes as reported by Aselage and Tissot [8] is included. We see that the samples measured in this investigation are all nearly fully dense. Specimens were prepared by cutting with a diamond saw. The samples were penny shaped with diameters of approximately 1 cm and thicknesses of approximately 1 mm. Before performing measurements, the thermal *diffusivities* above about 400 K were measured by Dr. C. Wood at the Jet Propulsion Laboratory (JPL) using a flash technique and then returned to Sandia for Raman spectroscopy to confirm that their carbon content had not changed as a result of the diffusivity measurements.

We employed the 3ω method, described in detail elsewhere [14], to measure thermal conductivity between 30 and 300 K. The 3ω method was developed to minimize errors due to thermal radiation which plague standard gradient techniques for measuring thermal conductiv-

TABLE 1. Mass densities and speeds of sound used for calculation of the Debye specific heat and Λ_{min} of $B_{1-x}C_x$. Measured sample densities [13] are compared with estimated theoretical densities for approximated isotopic composition of 100% ^{11}B and 100% ^{12}C using unit cell volumes reported by Aselage and Tissot [8]. Tabulated molar masses $\bar{M}$ assume 100% ^{11}B and 100% ^{12}C enrichment. Number densities of atoms obtained from ρ_{th} and $\bar{M}$ for each composition. Average room temperature speeds of sound measured by Gieske *et al.* [26] on a different set of boron carbides (but from the same boule as the samples measured in this investigation) with densities $\rho(x=0.1)=2.45$ g cm^{-3}, $\rho(x=0.133)=2.49$ g cm^{-3} and $\rho(x=0.2)=2.55$ g cm^{-3}. Debye speed of sound, v_D, calculated from longitudinal and transverse speeds of sound for each composition. Cut-off temperature $\theta_i=v_i(6\pi^2 n)^{1/3}(\hbar/k_B)$ for longitudinal and transverse phonon polarizations. Debye temperature $\theta_D=v_D(6\pi^2 n)^{1/3}(\hbar/k_B)$ calculated using tabulated values of v_D

	B_9C ($x=0.100$)	$B_{13}C_2$ ($x=0.133$)	B_4C ($x=0.200$)
ρ (g cm^{-3})	2.45	2.49	2.55
ρ_{th} (g cm^{-3})	2.48	2.50	2.55
m (g mol^{-1})	111.084	83.560	56.037
n (10^{23} cm^{-3})	1.34	1.35	1.37
v_l (10^5 cm s^{-1})	12.098	13.934	14.184
v_t (10^5 cm s^{-1})	7.342	8.723	8.851
v_D (10^5 cm s^{-1})	8.113	9.608	9.752
θ_l (K)	1843	2128	2177
θ_t (K)	1119	1332	1358
θ_D (K)	1236	1467	1497

ities of amorphous solids above about 100 K. This a.c. technique derives its name from the measurement of the third harmonic of voltage across a quasi-one-dimensional metal heater–thermometer which is heated by a current at angular frequency ω. This line is deposited (with contact pads for current and voltage leads) on the surface of the sample to be measured and is patterned either photolithographically or by evaporation through a shadow mask. Joule heating of the line generates a cylindrically symmetric thermal wave which diffuses into the sample. This wave is exponentially damped in the radial direction away from the 3ω line and has a frequency-dependent penetration depth δ of magnitude $\delta=(D/2\omega)^{1/2}$, where D is the thermal diffusivity of the underlying substrate. The I^2R heating of the 3ω line causes its temperature to oscillate at 2ω, thereby giving its electrical resistance the same frequency dependence. The net voltage drop across the metal line will therefore have a small component which oscillates at 3ω. The in-phase (real part) r.m.s. value of this voltage $V_{3\omega}$ varies with frequency and can be measured with a lock-in amplifier. The resulting analysis shows that the thermal conductivity can be determined from the frequency dependence of $V_{3\omega}$ via the relation [14]

$$\Lambda=\frac{I^3R}{4\pi l}\left(\frac{\ln(f_2)-\ln(f_1)}{V_{3\omega,1}-V_{3\omega,2}}\right)\frac{dR}{dT} \quad (1)$$

where I is the r.m.s. current through the metal line, R is its average resistance and l is its length. $V_{3\omega,1}$ and $V_{3\omega,2}$ are the r.m.s. $V_{3\omega}$ voltages measured at two different frequencies f_1 and f_2 and dR/dT is the derivative of the resistance *vs.* temperature calibration of the metal line. Experimentally we measure $V_{3\omega}$ at several frequencies and thereby extract the thermal conductivity of the sample by measuring the slope of such a frequency scan on a semilogarithmic plot. In this case we replace the bracketed ratio in eqn. (1) by the inverse of this slope. This tends to minimize the scatter in the resulting $\Lambda(T)$ data.

Because our samples are electrically conducting, it was necessary to electrically insulate the metal line from the substrate. This was done by coating the sample surface with a dilute solution of General Electric 7031 insulating varnish and thinner. The sample was inclined at approximately 45° and the solution was poured over the surface. The excess was blotted away from its edge and the coating was cured under a heat lamp for about 8 h. This procedure produces films less than 10 μm in thickness. Because these were bulk samples, it was sufficient to pattern the 3ω line on their surfaces by thermally evaporating 100 Å of NiCr (for improved adhesion) and 2000 Å of Ag through a shadow mask fashioned out of two nearly touching razor blades. The blades were aligned under an optical microscope. This technique produced lines 20–30 μm in width and about 4 mm in length, with room temperature electrical resistances of 10–80 Ω. Electrical contact to the current and voltage pads was achieved using four spring-loaded, gold-plated pins.

A typical frequency scan showing the magnitude of the in-phase voltage as a function of frequency is shown in Fig. 1. At low frequencies the penetration depth of the thermal wave is much larger than the thickness of the insulating layer and the slope of the frequency trace in this limit is inversely proportional to the thermal conductivity of the substrate. At higher frequencies the 3ω wave is rapidly damped out within the varnish layer and the assumption of cylindrical heat flow breaks down as the penetration depth of the 3ω wave becomes comparable with the width of the 3ω line. It is therefore not meaningful to extract a thermal conductivity for the varnish in this case. There is a smooth transition between the two regimes at intermediate frequencies. The upward trend in the signal at the highest frequencies is due to phase shifts introduced by the electronics. However, we note that the 3ω method has been successfully used to measure thermal conductivities of films with thicknesses $t>10$ μm [15]. Such films require photolithographically patterned heater–thermometer lines of widths about 2 μm. From the position of the knee in the frequency trace of Fig. 1 and an estimate of the thermal diffusivity of the varnish layer, we estimate the insulator thickness to be about 6 μm. The sample

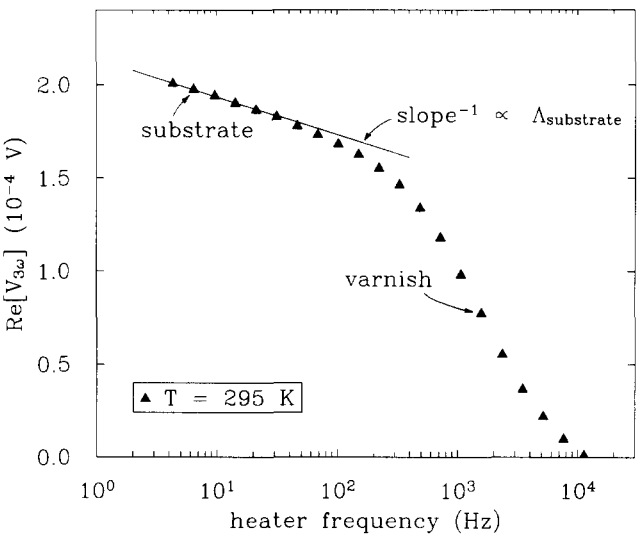

Fig. 1. Typical frequency scan for $x=0.133$ sample ($B_{13}C_2$) coated with GE 7031 varnish showing real part of 3ω voltage as a function of excitation frequency. At low frequencies ($\omega/2\pi<40$ Hz) the penetration depth of the thermal wave is much larger than the varnish thickness and thus we probe the $B_{13}C_2$ substrate to measure 5.1×10^{-2} W cm^{-1} K^{-1} as the thermal conductivity of the sample. For frequencies above about 800 Hz the thermal wave is damped out within the varnish layer (see text).

temperature was varied between 30 and 300 K using an insertion-type ^{4}He cryostat [16].

3.2. Specific heat

Measurements of specific heat for $80 < T < 300$ K were performed using a diffusive heat pulse technique as described by Fischer *et al.* [17]. In this method a voltage pulse is applied to an evaporated thin film heater which nearly covers one side of a penny-shaped sample. A small, thin film bolometer is evaporated on the opposite face of the sample. The time dependence of the bolometer's temperature rise allows one to extract the heat capacity and thermal diffusivity of the sample. Knowledge of the sample's mass density then permits calculation of its thermal conductivity via the relation

$$D = \frac{\Lambda}{\rho C_p} \tag{2}$$

where D is the thermal diffusivity, Λ is the thermal conductivity, ρ is the mass density and C_p is the specific heat per unit mass (at constant pressure). The $B_{1-x}C_x$ samples measured using this heat pulse technique were the same ones measured by Türkes *et al.* [18] and are described in that reference. The specific heat measurements reported by Türkes *et al.* below 100 K were performed using an adiabatic calorimeter method as described in detail elsewhere [16]. They also measured thermal conductivities below 100 K using a steady state heat flow (gradient) technique.

4. Experimental results

4.1. Specific heat

The specific heat data [18–23] presented in Fig. 2 span a wide range of carbon compositions, preparation methods, morphologies and measurement techniques. Between about 60 and 1000 K the specific heat is essentially independent of carbon concentration x. At lower temperatures (not shown here) the specific heats fail to follow this common behavior. Fischer *et al.* have shown that low temperature specific heat anomalies observed in certain boron carbide specimens are extrinsic in origin [17]. However, it is the $T > 60$ K data which will be relevant to the interpretation of the high temperature thermal conductivity and thermal diffusivity. In this regime we believe that the measured specific heats are intrinsic. The independence of the specific heat on x suggests that the phonon frequencies and their density of states are essentially insensitive to the amount of carbon in the lattice. For the carbon-rich samples the average atomic mass is higher and we might expect to have lower vibrational frequencies on average in these samples, all other things being equal. This would lead to a higher specific heat at a given temperature for the carbon-rich samples. However, if the carbon–boron (C–B) bond is stronger than the boron–boron (B–B) bond, this might compensate for the frequency reduction due to the higher atomic mass of the carbon. There is evidence to support this idea. Raman peaks associated with the intericosahedral three-member chains in $B_{1-x}C_x$ show a shift to lower frequencies as CBC chains are converted to CBB chains for carbon-deficient compositions [24]. X-Ray measurements show that the $B_{1-x}C_x$ rhombohedral unit cell elongates along its body diagonal as carbon is removed [25]. However, this elongation is believed to reflect only increases in the length of direct bonds between icosahedra (along the rhombohedral cell edges) and increases in intraicosahedral bond lengths. These changes are thought to be due to the removal of bonding electrons as boron substitutes for carbon in carbon-deficient specimens. The elongation of the rhombohedral cell does not appear to be due to a lengthening of the intericosahedral chains themselves [8]. We will

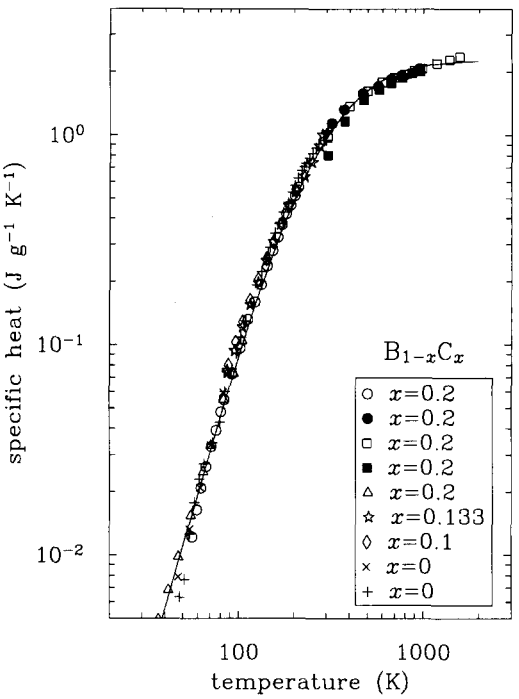

Fig. 2. Specific heat of $B_{1-x}C_x$ and β-B ($x=0$). Data for $x=0.2$ samples: granular, crystalline specimen (96% B_4C, 4% free and included graphite) due to Kelley [19] (open circles); hot-pressed specimen due to Gilchrist and Preston [20] (solid circles); granular, crystalline specimen (similar to Kelley's above) due to King [21] (open squares); specimen of unknown morphology due to Scheindlin *et al.* [22] (solid squares); sample GA 8798-95-2 due to Türkes *et al.* [18] (open triangles). Data for hot-pressed $x=0.133$ and 0.1 specimens: this investigation (open stars, open diamonds). Data for β-B: single-crystal specimen seed pulled from the melt due to Türkes *et al.* [18] (×); sample vacuum hot pressed from amorphous boron powder due to Johnston *et al.* [23] (+). The solid curve is the calculated specific heat of B_9C in the Debye approximation (see text).

see later that these observations are consistent with the structural changes in the rhombohedral cell which are believed to occur as the carbon content of the lattice is varied.

The solid curve in Fig. 2 is the calculated specific heat for B_9C ($x = 0.1$) in the Debye approximation based upon ultrasonic measurements of its room temperature sound speeds [26] (see Table 1). The values of v_l and v_t in Table 1 are averages for B_9C samples of various thicknesses measured by Gieske *et al.* [26]. The samples in that study and the samples in this work were from the same boules. For calculational purposes we therefore take $\rho = 2.48$ g cm^{-3} and assume that the tabulated v_l and v_t are reasonable approximations to their low temperature values. This yields a Debye velocity and temperature of $v_D = 8.1 \times 10^5$ cm s^{-1} and $\theta_D = v_D(6\pi^2 n)^{1/3}(\hbar/k_B) = 1236$ K respectively using $n = 1.34 \times 10^{23}$ cm^{-3} for the number density of atoms and $\hbar = h/2\pi$, where h is Planck's constant and k_B is Boltzmann's constant. We see that the theoretical curve agrees quantitatively well with all the data. In addition to the independence of the specific heat on x over the single-phase field, it is remarkable that the boron carbide specific heats are also in good agreement with data for β-B hot pressed from amorphous boron powder (data due to Johnston *et al.* [23]) and single-crystal β-B seed pulled from the melt (data due to Türkes *et al.* [18]). The crystal structure of β-B is distinct from that of α-B and therefore also from the boron carbides whose structure is a modification of the α-B lattice. The universality of the high temperature specific heats of boron carbides is in stark contrast with the disaccord amongst their thermal conductivities. We now turn to this subject.

4.2. Thermal diffusivity and conductivity

The high temperature ($T > 400$ K) thermal diffusivities of $B_{1-x}C_x$ measured by Wood are shown in Fig. 3 [11]. Over the entire temperature range the diffusivity decreases as carbon is removed from the lattice. The increased amount of scatter in the data for the $x = 0.192$ sample above about 950 K suggests that those data should be viewed cautiously. We have seen above that C_p is essentially independent of x for $T > 60$ K. Because the thermal diffusivity is directly proportional to the thermal conductivity by eqn. (2), any variation in D should therefore be observed in Λ above about 60 K. We sought to confirm the compositional trend observed in the diffusivity measurements (Fig. 3) by measuring the thermal *conductivity* of Wood's samples at lower temperatures ($30 < T < 300$ K) using the 3ω method.

Figure 4 shows the thermal conductivity. The variation in the $T > 400$ K thermal diffusivities with x is also present in the thermal conductivities at lower temperatures ($T < 300$ K). As the carbon content of the

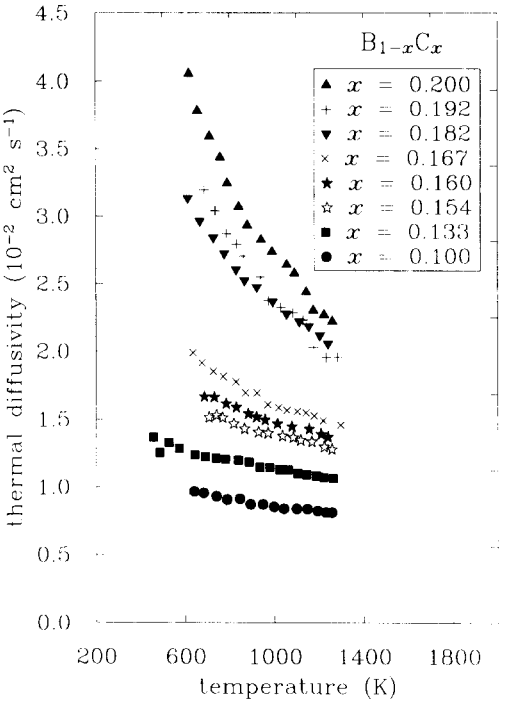

Fig. 3. Thermal diffusivity of $B_{1-x}C_x$ for various values of x as measured by Wood [11]. All specimens were hot pressed at Sandia National Laboratories. The $x = 0.2$, 0.133 and 0.1 samples are the same ones measured in this investigation using the 3ω method.

lattice decreases, so does Λ. Also shown for comparison are previous low temperature ($T < 100$ K) thermal conductivity measurements (using a standard gradient technique) on different samples [18] due to Türkes *et al.* (open symbols below 100 K). In addition, we compare our results with values of the thermal conductivity calculated from Wood's thermal diffusivity measurements (Fig. 3) using the average fit to the specific heat data described above (Fig. 2) and the appropriate sample density (open symbols above 400 K). The consistency of the data between the *same* samples and even between entirely *different* samples of nominally identical stoichiometry is striking. The additional fact that these data were all taken using different measurement techniques gives us confidence that the measured thermal conductivities are indeed intrinsic.

The solid squares in Fig. 4 are the results for our $x = 0.2$ sample (corresponding to the chemical formula B_4C) using the 3ω technique. They agree well with Türkes *et al.*'s low temperature measurements [18] on a different sample of B_4C (arc-melted ingot) obtained from Elektroschmelzwerk Kempten (ESK). Our data for B_4C extrapolate well to the high temperature ($T > 400$ K) thermal conductivity, thereby giving us confidence in the quality of the data. The presence of a peak at about 60 K and the decreasing thermal conductivity above this temperature indicate that the thermal trans-

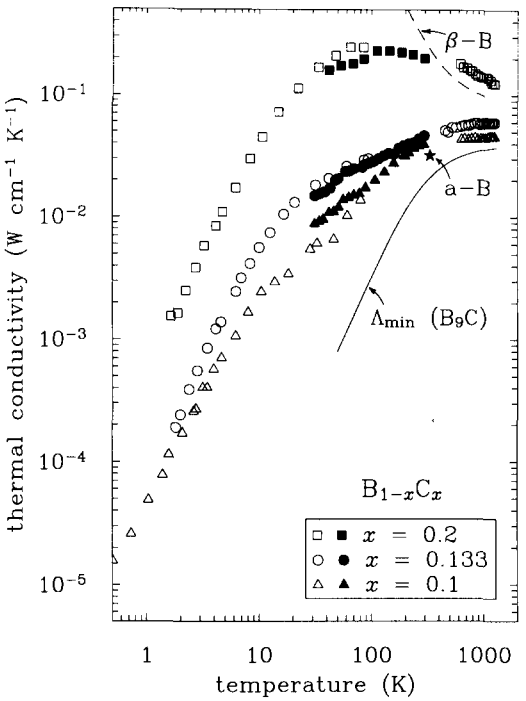

Fig. 4. Thermal conductivity of $B_{1-x}C_x$. All solid symbols: hot-pressed samples from Sandia, this investigation, $x=0.2$, 0.133 and 0.1. Open symbols above about 400 K: thermal conductivities derived from thermal diffusivity data in Fig. 3 due to Wood (see text). Open symbols below about 100 K [18]: $x=0.2$ arc-melted ingot from ESK; $x=0.133$ reactively hot-pressed sample GA 8798-92-1; $x=0.1$ reactively hot-pressed sample GA 8235-147-2. Single data point for amorphous B due to Talley *et al.* [32] (★). β-B single-crystal specimen due to Golikova *et al.* [34] (dashed curve below 1000 K). Λ_{min} curve: theoretical minimum thermal conductivity of B_9C (solid curve, see text).

port in B_4C is indeed crystal like, although because of the low magnitude and weak temperature dependence of the conductivity, it appears that there is some disorder which scatters the phonons in the lattice (compare with the dashed curve for the probably more perfect crystalline β-B). It is possible that this scattering is partially due to the presence of a small amount of free carbon in the sample, since the measured carbon content ($x=0.2$) slightly exceeds the proposed carbon solubility limit ($x=0.2-\epsilon$, $\epsilon \ll 1$). We dismiss the possibility of scattering from grain boundaries or voids as will be discussed below.

As reported in previous studies [17], the character of the thermal transport changes greatly once carbon is removed from the lattice. The solid circles are results for our sample of $B_{13}C_2$ ($x=0.133$). Note that the conductivity at room temperature is a factor of about 4 below that of B_4C. There is no longer a peak in the thermal conductivity as there was for B_4C. Our results join on smoothly to Türkes *et al.*'s low temperature measurements [18] on a different sample (reactively hot pressed at General Atomics, sample number GA 8798-92-1) of $B_{13}C_2$ and also extrapolate nicely to the high temperature thermal conductivity (open circles) derived from Wood's diffusivity data. Both the magnitude and temperature dependence of the composite data for $B_{13}C_2$ suggest the beginnings of a transition to a conductivity characteristic of an amorphous solid, although certain features such as the presence of a well-defined plateau are absent.

Further reduction of x causes the thermal conductivity to continue to depart from crystalline behavior in both magnitude and temperature dependence. Our results for B_9C ($x=0.1$) match up reasonably well with the low temperature measurements [18] on a different sample (reactively hot pressed at General Atomics, sample number 8235-147-2) and with Wood's high temperature data. The important point is that the thermal conductivity has continued to decrease below that of $B_{13}C_2$. In contrast, Bouchacourt and Thevenot [3] concluded that the thermal conductivity decreases with carbon concentration and reaches a minimum at $x=0.133$, beyond which it rises again. In an earlier study [27] using different samples, Wood *et al.* had also observed some evidence for a minimum in the thermal diffusivity at high temperatures, although there was considerable scatter in the data. We see no such evidence for a minimum in the thermal conductivity or thermal diffusivity data presented here. Our data in this investigation show remarkably little dependence on sample origin and we therefore believe that the measured thermal conductivities are intrinsic. Because of this, we suggest that earlier discrepancies in transport data were due to measurement technique. We therefore wish to stress that the data presented in this work complete our knowledge of thermal transport in boron carbides over several orders of magnitude in temperature.

We submit that any effects on the thermal conductivity due to grain boundaries are negligible over the temperature range from about 30 to 300 K, since the phonon mean free path is much smaller than the size of the grains in this temperature regime. In order to see this, consider the expression for the thermal conductivity obtained by treating thermal transport as the diffusion of a phonon gas using the kinetic theory:

$$\Lambda = \tfrac{1}{3} C_v \rho v \bar{l} \qquad (3)$$

where C_v is the specific heat (per unit mass), ρ is the mass density, v is the average sound velocity and $\bar{l}$ is the average mean free path. Using the specific heat and thermal conductivity data presented here, we estimate average mean free paths of 2×10^{-3} and 0.1 μm at 300 and 60 K respectively for B_4C. This is much smaller than the lower limit of 10 μm for the grain size of this sample. The average mean free paths are even smaller for samples with lower carbon content. We estimate 7×10^{-4} and $(1\text{–}2)\times10^{-2}$ μm at 300 and

60 K respectively for $B_{13}C_2$ and B_9C. We conclude that the thermal conductivity is unaffected by scattering from grain boundaries for $T > 60$ K. It is also clear that this must be the case since such an extrinsic effect would not be consistent with the observed agreement between the measured thermal conductivities of samples with widely different origins and process histories.

In addition, because all samples studied have densities in excess of 98% of their estimated theoretical values, the existence of voids within grains, which could significantly affect the thermal conductivity, appears to be precluded. This statement is also supported by the observed agreement between the data for all samples shown in Fig. 4. Theoretical models of electrical conduction in discontinuous networks [28] have been shown to agree with the observed temperature-independent reduction of thermal conductivity in porous media such as Vycor glass [29]. Such models predict a negligible effect on the thermal conductivity in highly dense samples such as those studied here.

Also shown in Fig. 4 are calculations of the theoretical minimum thermal conductivity (Λ_{min}) for a material with the composition B_9C. This is based upon a model originally due to Einstein to explain the thermal conductivity of crystalline solids [30]. The model, subsequently modified by Cahill and Pohl [31], treats thermal transport in amorphous solids and certain disordered crystals at high temperatures as a random walk of energy amongst weakly coupled, highly damped oscillators which have uncorrelated phases. These microscopic oscillators are individual atoms or small groups of atoms which transfer thermal energy to their neighbors within approximately one-half of their vibrational period. The lack of phase correlation precludes the existence of collective wave-like energy transport (*i.e.* phonons) and the model therefore failed in its original aim to explain the thermal conductivity of crystals. However, it appears to have some applicability to the high temperature thermal conductivity of amorphous solids and some disordered crystals [31].

For the calculation of Λ_{min} for a substance of the chemical composition B_9C, we used the number density of atoms $n = 1.34 \times 10^{23}$ cm^{-3} and the average room temperature sound speeds $v_l = 1.2 \times 10^6$ cm s^{-1} and $v_t = 7.3 \times 10^5$ cm s^{-1} (see Table 1). As observed for *amorphous* solids, the calculated conductivities fall off much faster than the actual data at lower temperatures. This is expected because this theory does not include the contribution of long wavelength phonons which must exist at low temperatures. Note that there are no free parameters in the expression for Λ_{min}; we only require knowledge of the speed of sound and number density of atoms. In light of this, the calculated Λ_{min} values agree remarkably well with the data as expected in the high temperature limit. In addition, the calculated Λ_{min} for B_9C is close to the single data point for an amorphous boron sample reported by Talley *et al.* [32]. However, the microscopic details of such a transport model are not clear, because peaks in the Raman and IR spectra of these materials are sharp. They do not exhibit significant broadening as would be expected for highly damped oscillators [33].

We now consider the interpretation of the thermal conductivity in terms of the microscopic variation in site occupancy of the boron carbide lattice as a function of carbon content. Emin has developed such a picture in a effort to explain the observed structural, electronic and thermal properties [11]. At the carbon-saturated limit of the phase field the only form of disorder in the lattice is the random placement of the single carbon atom within the icosahedra. Apart from this disorder, the lattice is ordered. This is reflected in the thermal conductivity, which resembles that of a crystalline solid.

For carbon-deficient specimens the conversion of CBC chains to CBB chains continues until the composition $x = 0.133$, at which point all the intericosahedral chains have been converted to the CBB configuration. Recall that the thermal conductivity and thermal diffusivity begin to show departure (in magnitude and temperature dependence) from crystalline behavior for $x < 0.2$, although it is not clear at precisely which value of x the thermal transport exhibits this transition. This may be a reflection of the random placement of CBC and CBB chains within the lattice in this region of the phase field. Continued removal of carbon from the icosahedra is accompanied by further reduction in the thermal conductivity over a wide range of temperature. Most noteworthy is the fact that it approaches both a magnitude and temperature dependence which is characteristic of amorphous solids. In particular, the similarity in the magnitude of thermal conductivity for carbon-poor $B_{1-x}C_x$ and the single data point shown for a-B suggests that the minimum thermal conductivity for single-phase boron carbides is nearly that of bulk amorphous boron.

In Emin's theory [11], *electrical* conduction in boron carbides occurs via phonon-assisted hopping of singlet bipolaronic holes which are localized on inequivalent icosahedra. In analogy with this idea, Emin has posited a hopping type of thermal conduction in which the predominant transport of energy is through the intericosahedral chains [33]. In this picture the central atom of the chain provides weak coupling between anharmonic oscillators localized at the ends of the chains. One possible choice for such a vibrational unit would be the end atom of a chain and the three icosahedral atoms to which it is bonded. The vibrations of these relatively stiff end-chain units depend upon the atoms in the unit and their bonding with one another. As the carbon content of the lattice is varied, electrons

are removed from icosahedral bonding orbitals and the vibrational frequencies of these units will therefore shift. If the frequencies of two vibrational units at either end of a chain are sufficiently disparate, no energy will be transferred between the two. In particular, for carbon-poor boron carbides, different types of atoms reside at opposite ends of the CBB chains for $x<0.133$. As the carbon concentration is lowered even further, the bonding of these end-chain atoms to icosahedral atoms changes. This is because intraicosahedral bonding orbitals are gradually depleted of electrons in carbon-deficient specimens. Using the structural model of Emin, we expect an increasing disparity in the frequencies of the end-chain vibrational units as the carbon-poor phase boundary is approached. One would therefore also expect a decreasing thermal diffusivity with decreasing carbon content [11] in agreement with this work.

5. Conclusions

Reliable data of thermal conductivity, thermal diffusivity and specific heat capacity for $B_{1-x}C_x$ now exist over a wide temperature range for specimens spanning the single-phase field ($0.1<x<0.2$). The specimens examined have different origins and modes of preparation. In addition, various measurement techniques were used in different temperature regimes. The consistency of the data amongst all these efforts indicates that the observed behavior is indeed intrinsic to $B_{1-x}C_x$ and permits several conclusions. First, the specific heat is *independent* of carbon concentration for $T>60$ K. Measurements of the specific heat at low temperatures ($T<60$ K) exhibit anomalies which have been shown to be extrinsic in origin. Secondly, at the carbon-rich end of the phase field the thermal conductivity is characteristic of a crystal in temperature dependence, indicative of thermal transport via phonons. The conductivity shows signs of defect scattering, indicative of some disorder. It is possible that this scattering is caused by the presence of a small amount of free carbon in the $x=0.2$ sample rather than scattering from grain boundaries or voids. For carbon-deficient samples ($x<0.2$) the thermal conductivity decreases in magnitude and evolves into behavior characteristic of an amorphous solid. The measured thermal conductivity for the $x=0.1$ sample is the lowest of all and has a magnitude near that of amorphous boron. In particular, there is no evidence for a minimum in the thermal conductivity at an intermediate carbon concentration $x\approx0.133$ as claimed by other researchers. The observed continuous decrease in thermal conductivity here is mirrored by a similar trend in measurements of thermal diffusivity at high temperatures ($T>400$ K). Our results are in good agreement with these high temperature measurements after an appropriate conversion using known specific heat and density data.

Acknowledgments

Stimulating discussions with Drs. D. Emin, T. Aselage and other members of the boron carbide group at Sandia National Laboratories are gratefully acknowledged.

This work was supported by the National Science Foundation (Grant Number DMR-91-15981), Sandia National Laboratories under Contract Number 42-6392 and through the Cornell Materials Science Center.

References

1 M.L. Wilkins, in V.I. Matkovich (ed.), *Boron and Refractory Borides,* Springer, New York, 1977, p. 633.
2 D.E. Mahagin and R.E. Dahl, in V.I. Matkovich (ed.), *Boron and Refractory Borides,* Springer, New York, 1977, p. 613.
3 M. Bouchacourt and F. Thevenot, *J. Mater. Sci., 20* (1985) 1237.
4 T.B. Massalski, J.L. Murray, L.H. Bennet and H. Baker (eds.), *Binary Alloy Phase Diagrams,* American Society for Metals, Metals Park, OH, 1986, p. 465.
5 M. Bouchacourt and F. Thevenot, *J. Less-Common Met., 82* (1981) 219.
6 K.A. Schwetz and P. Karduck, *AIP Conf. Proc., 231* (1991) 405.
7 H.K. Clark and J.L. Hoard, *J. Am. Chem. Soc., 65* (1943) 2115.
8 T.L. Aselage and R.G. Tissot, *J. Am. Ceram. Soc., 75*(8) (1992) 2207.
9 T.L. Aselage and D. Emin, *AIP Conf. Proc., 231* (1991) 177.
10 D. Emin, *Phys. Rev. B, 38* (1988) 6041.
11 D. Emin, in R. Freer (ed.), *The Physics and Chemistry of Carbides, Nitrides, and Borides,* Kluwer, Dordrecht, 1990, p. 691.
12 T.L. Aselage, D.R. Tallant, J.H. Gieske, S.B. Van Deusen and R.G. Tissot, in R. Freer (ed.), *The Physics and Chemistry of Carbides, Nitrides, and Borides,* Kluwer, Dordrecht, 1990, p. 97.
13 T.L. Aselage, personal communication, 1993.
14 D.G. Cahill, *Rev. Sci. Instrum., 61*(2) (1990) 802.
15 D.G. Cahill, H.E. Fischer, T. Klitsner, E.T. Swartz and R.O. Pohl, *J. Vac. Sci. Technol. A, 7*(3) (1989) 1259.
16 E.T. Swartz, *Rev. Sci. Instrum., 57*(11) (1986) 2848.
17 H.E. Fischer, E.T. Swartz, P.R.H. Türkes and R.O. Pohl, *MRS Symp. Proc., 97* (1987) 69.
18 P.R.H. Türkes, E.T. Swartz and R.O. Pohl, *AIP Conf. Proc., 140* (1986) 346.
19 K.K. Kelley, *J. Am. Chem. Soc., 63* (1941) 1137.
20 K.E. Gilchrist and S.D. Preston, *High Temp.–High Press., 11* (1979) 643.
21 E.G. King, *Ind. Eng. Chem., 41* (1949) 1298.
22 A.E. Sheindlin, I.S. Belevich and I.G. Kozhevnikov, *High Temp., 10* (1972) 369.
23 H.L. Johnston, H.N. Hersh and E.C. Kerr, *J. Am. Chem. Soc., 73* (1951) 1112.
24 D.R. Tallant, T.L. Aselage, A.N. Campbell and D. Emin, *Phys. Rev. B, 40* (1989) 5649.

25 B. Morosin, A.W. Mullendore, D. Emin and G.A. Slack, *AIP Conf. Proc., 140* (1986) 70.
26 J.H. Gieske, T.L. Aselage and D. Emin, *AIP Conf. Proc., 231* (1991) 376.
27 C. Wood, D. Emin and P.E. Gray, *Phys. Rev. B, 31* (1985) 6811.
28 S. Kirkpatrick, *Rev. Mod. Phys., 45* (1973) 574.
29 D.G. Cahill, R.B. Stephens, R.H. Tait, S.K. Watson and R.O. Pohl, in C.J. Cremers and H.A. Fine (eds.), *Thermal Conductivity 21,* Plenum, New York, 1990, p. 3.
30 A. Einstein, *Ann. Phys., 35* (1911) 679.
31 D.G. Cahill and R.O. Pohl, *Solid State Commun., 70* (1989) 927.
32 C.P. Talley, L.E. Line Jr. and Q.D. Overman Jr., in J.A. Kohn, W.F. Nye and G.K. Gaulé (eds.), *Boron: Synthesis, Structure, and Properties,* Plenum, New York, 1960, p. 94.
33 D. Emin, personal communication, 1993.
34 O.A. Golikova, V.K. Zaitsev, V.M. Orlov, A.V. Petrov, L.S. Stilbans and E.N. Tkalenko, *Phys. Status Solidi A, 21* (1974) 405.